The Astrophysical Journal, 649: L67–L70, 2006 October 1
© 2006. The American Astronomical Society. All rights reserved. Printed in U.S.A.

SPITZER IRAC CONFIRMATION OF z_{850}-DROPOUT GALAXIES IN THE HUBBLE ULTRA DEEP FIELD: STELLAR MASSES AND AGES AT $z \approx 7$[1]

Ivo Labbé,[2,3] Rychard Bouwens,[4] G. D. Illingworth,[4] and M. Franx[5]

Received 2006 May 26; accepted 2006 August 18; published 2006 September 18

ABSTRACT

Using *Spitzer* IRAC mid-infrared imaging from the Great Observatories Origins Deep Survey, we study z_{850}-dropout sources in the Hubble Ultra Deep Field. After carefully removing contaminating flux from foreground sources, we clearly detect two z_{850} dropouts at 3.6 and 4.5 μm, while two others are marginally detected. The mid-infrared fluxes strongly support their interpretation as galaxies at $z \approx 7$, seen when the universe was only 750 Myr old. The IRAC observations allow us for the first time to constrain the rest-frame optical colors, stellar masses, and ages of the highest redshift galaxies. Fitting stellar population models to the spectral energy distributions, we find photometric redshifts in the range 6.7–7.4, rest-frame colors $U - V = 0.2$–0.4, V-band luminosities $L_V = (0.6\text{–}3) \times 10^{10}\, L_\odot$, stellar masses $(1\text{–}10) \times 10^9\, M_\odot$, stellar ages 50–200 Myr, star formation rates up to $\sim 25\, M_\odot\ \mathrm{yr}^{-1}$, and low reddening $A_V < 0.4$. Overall, the $z = 7$ galaxies appear substantially less massive and evolved than Lyman break galaxies or distant red galaxies at $z = 2$–3, but fairly similar to recently identified systems at $z = 5$–6. The stellar mass density inferred from our $z = 7$ sample is $\rho_* = 1.6^{+1.6}_{-0.8} \times 10^6\, M_\odot\ \mathrm{Mpc}^{-3}$ (to $0.3 L^*_{z=3}$), in apparent agreement with recent cosmological hydrodynamic simulations, but we note that incompleteness and sample variance may introduce larger uncertainties. The ages of the two most massive galaxies suggest that they formed at $z \gtrsim 8$, during the era of cosmic reionization, but the star formation rate density derived from their stellar masses and ages is not nearly sufficient to reionize the universe. The simplest explanation for this deficiency is that lower mass galaxies beyond our detection limit reionized the universe.

Subject headings: galaxies: evolution — galaxies: high-redshift — infrared: galaxies

1. INTRODUCTION

Observations of massive galaxies at high redshift with the *Hubble Space Telescope* and the *Spitzer Space Telescope* are revolutionizing our knowledge of the early formation history of stars and galaxies. Blue star-forming galaxies at $z = 2$–3 with stellar masses 10^{10}–$10^{11}\, M_\odot$ are routinely identified from optical imaging (Steidel et al. 1996a, 1996b, 2004) and have been studied in detail (e.g., Papovich et al. 2001; Shapley et al. 2001, 2005), while near-infrared surveys at $z = 2$–3 have uncovered substantial numbers of redder, more evolved galaxies with larger stellar masses $>10^{11}\, M_\odot$ (Franx et al. 2003; Yan et al. 2004; Daddi et al. 2005). Some of these red galaxies appear to have stellar ages >1.5 Gyr, implying that they formed most of their stars before $z \sim 5$ (Labbé et al. 2005), and suggesting that massive galaxies should exist well beyond these redshifts. Direct detection of such galaxies would place strong constraints on galaxy formation models (e.g., Somerville et al. 2001; Nagamine et al. 2005).

Tantalizingly, the most recent surveys with the Advanced Camera for Surveys (ACS) and the Near-Infrared Camera and Multiobject Spectrograph (NICMOS) on the *Hubble Space Telescope* have identified sources at $z = 5$–6.5 with fairly evolved stars and stellar masses of $(1\text{–}4) \times 10^{10}\, M_\odot$ (e.g., Yan et al. 2005; Eyles et al. 2005; Dow-Hygelund et al. 2005) or perhaps more (Mobasher et al. 2005). Critical to these results was access to the rest-frame wavelengths longward of the Balmer/4000 Å break offered by the Infrared Array Camera (IRAC; Fazio et al. 2004) on *Spitzer*. Without mid-infrared photometry to very faint magnitudes, the stellar ages and masses of $z \gtrsim 5$ galaxies are poorly constrained.

In this Letter, we extend mass estimates to $z = 7$–8 by analyzing the mid-infrared fluxes of six z_{850}-dropout candidates found in the Hubble Ultra Deep Field (HUDF) by Bouwens et al. (2004, hereafter B04). These candidates were selected from exceptionally deep optical ACS (S. V. W. Beckwith et al. 2006, in preparation) and near-infrared NICMOS imaging (Thompson et al. 2005), and when combined with the ultradeep IRAC data available there, offer us an ideal opportunity to verify their reality and to study their stellar populations. The stellar masses and ages of z_{850}-dropout galaxies would provide us with the first direct look at galaxy formation at $z \gtrsim 7$, building on the comprehensive $z \sim 6$ study (Bouwens et al. 2006b). Where necessary, we assume an $\Omega_M = 0.3$, $\Omega_\Lambda = 0.7$ cosmology with $H_0 = 70\ \mathrm{km\ s^{-1}\ Mpc^{-1}}$. Magnitudes are expressed in the AB photometric system.

2. OBSERVATIONS

The Great Observatories Origins Deep Survey (GOODS; M. Dickinson et al. 2006, in preparation) observed the HUDF with IRAC in two epochs, each time integrating for ≈23.3 hr in the 3.6, 4.5, 5.8, and 8.0 μm channels.[6] We estimate limiting depths in the combined IRAC images by measuring the effective flux variation in random apertures on empty background

[1] Based on observations with the *Spitzer Space Telescope*, which is operated by the Jet Propulsion Laboratory, California Institute of Technology under NASA contract 1407. Support for this work was provided by NASA through contract 125790 issued by JPL/Caltech. Based on observations with the NASA/ESA *Hubble Space Telescope*, obtained at the Space Telescope Science Institute, which is operated by the Association of Universities for Research in Astronomy, Inc., under NASA contract NAS5-26555. Based on service mode observations collected at the European Southern Observatory, Paranal, Chile (ESO program 073.A-0764A).

[2] Carnegie Observatories, 813 Santa Barbara Street, Pasadena, CA 91101; ivo@ociw.edu.

[3] Carnegie Fellow.

[4] UCO/Lick Observatory, Department of Astronomy and Astrophysics, University of California Santa Cruz, Santa Cruz, CA 95064.

[5] Leiden Observatory, Postbus 9513, 2300 RA Leiden, Netherlands.

[6] This Letter uses Data Release 3 of epoch 1 and Data Release 2 of epoch 2, available from http://data.spitzer.caltech.edu/popular/goods/.

TABLE 1
CORRECTED PHOTOMETRY OF z_{850}-DROPOUTS IN THE HUDF

ID	z_{850}	J_{110}	H_{160}	K_s	3.6 μm	4.5 μm
964	>29.6	26.8 ± 0.2	26.8 ± 0.2	27.0 ± 0.9	26.1 ± 0.2	26.4 ± 0.5
1417	28.0 ± 0.2	26.7 ± 0.2	26.3 ± 0.2	26.1 ± 0.3	25.3 ± 0.1	25.5 ± 0.2
950	>29.6	26.9 ± 0.2	26.6 ± 0.2	>27.2	27.0 ± 0.5	26.4 ± 0.5
1125	29.2 ± 0.7	27.3 ± 0.4	27.2 ± 0.3	>27.2	26.9 ± 0.4	>27.2

NOTES.—Object IDs are from B04. All magnitudes are in the AB system. Optical/near-infrared fluxes were measured in 0.″9 diameter apertures and IRAC fluxes were measured in 2.″5 diameter apertures. We corrected the fluxes for missing light outside the aperture assuming stellar profiles. The corrections are 5%–20% in the optical/near-infrared and a factor of 1.75 and 1.81 for IRAC 3.6 and 4.5 μm, respectively. We adjusted the NICMOS J_{110} and H_{160} zero points by -0.16 and -0.04 following de Jong et al. (2006). In the improved NICMOS reduction (B06) object 1417 falls within the z_{850}-dropout selection criteria, whereas in B04 it fell just outside. The upper limits are 1 σ. None of the galaxies are detected in V_{606}, i_{775}, and 5.8 μm to 1 σ limits of 30.6, 30.5, and 25.1, respectively.

regions. The limits for point sources are 27.7, 27.2, 25.1, and 24.9 in the four channels (1 σ, total, 2.″5 diameter aperture). We supplement the observations with deep K_s-band data from the Very Large Telescope and *Magellan* (I. Labbé et al. 2006, in preparation), and we use an independent reduction of HUDF NICMOS data with improved noise properties and fewer artifacts (Bouwens & Illingworth 2006, hereafter BI06). The new NICMOS images revealed that two of the original six z_{850} dropouts were electronic ghosts of nearby bright stars; hence, we removed them from the sample.

Matching ACS NICMOS and IRAC photometry is challenging because of the much larger size and extended wings of the IRAC point-spread functions (PSFs), resulting in flux contamination by nearby foreground sources. Visual inspection shows that two z_{850} dropouts are substantially blended, and all four are likely to contain at least some flux from nearby objects. We have developed a technique to robustly subtract the contaminating flux (I. Labbé et al. 2006, in preparation). Briefly, we first detect sources with SExtractor (Bertin & Arnouts 1996) in a summed NICMOS $J_{110} + H_{160}$ image to determine the light distributions at high resolution using the pixels in the "segmentation" maps. We then convolve these template images individually with a carefully constructed kernel to match it to the IRAC PSF. Third, we fit all detected sources, including neighbors, simultaneously to the registered IRAC image, leaving only the flux scalings as free parameters. Finally, we subtract the best-fit images of all neighboring sources.

After cleaning the IRAC images, we performed conventional aperture photometry in 3.6, 4.5, 5.8, and 8.0 μm bands in 2.″5 diameter apertures. Photometry in the ACS B_{435}, V_{606}, i_{775}, z_{850}, NICMOS J_{110}, H_{160}, and K_s bands was done in 0.″9 diameter apertures, and we obtained magnitudes and limits consistent with B04. We summarize the photometry in Table 1.

3. MID-INFRARED FLUXES OF z_{850}-DROPOUT SOURCES

Figure 1 shows the *HST* ACS+NICMOS and the combined *Spitzer* IRAC images of the z_{850} dropouts. Two objects (IDs 964 and 1417) are unambiguously detected in 3.6 μm (5–8 σ) and in the slightly shallower 4.5 μm (2–3 σ). Two others (IDs 950 and 1125) are only marginally detected but are probably real as the sum of their 3.6 and 4.5 μm images reveals a visible source. Unfortunately, the IRAC observations are not deep enough to definitively confirm or reject the reality of the undetected sources. None of the candidates are visible at 5.8 and 8.0 μm. To evaluate the robustness of the deblending photometry, we performed the procedure independently on the first- and second-epoch IRAC data (see Fig. 2). Reassuringly, we measure consistent fluxes, and we detect the brightest, most promising sources 964 and 1417 in each data set individually.

The 3.6 μm magnitudes are faint, ranging from 25.3 to 27.0, with $H_{160} - 3.6$ μm colors in the range -0.4 to 1.0. The IRAC-detected objects 964 and 1417 are the reddest, showing a factor of ~2 rise in f_ν flux densities between H_{160} and 3.6 μm, while

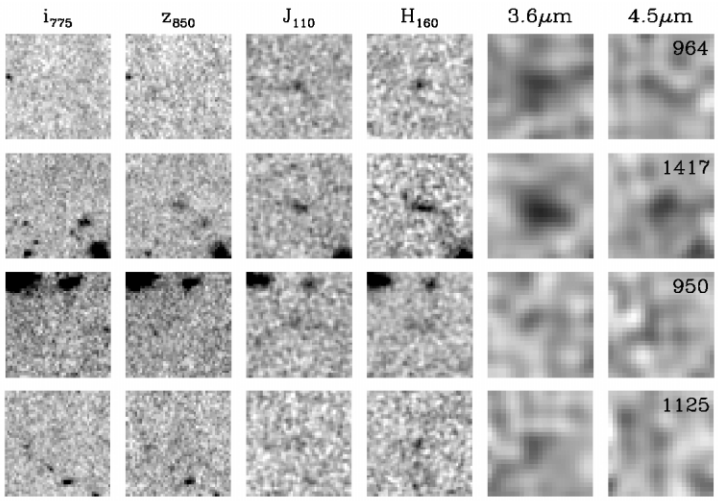

FIG. 1.—Images of z_{850} dropouts in the HUDF from *HST* ACS (i_{775}, z_{850}), NICMOS (J_{110}, H_{160}), and *Spitzer* IRAC (3.6 μm, 4.5 μm). All sources are undetected (<2 σ) at i_{775} and bluer wavelengths, but we note that z_{850}-dropout galaxies can have some flux at i_{775} due to incomplete absorption between Lyα at rest-frame 1216 Å and the Lyman limit at 912 Å. The top two candidates are clearly detected in the IRAC 3.6 and 4.5 μm images, while two others are marginally detected. Flux contribution from nearby sources was subtracted in the *Spitzer* images. Each panel is 4.″1 × 4.″1 in size, or ≈21 kpc at $z = 7$.

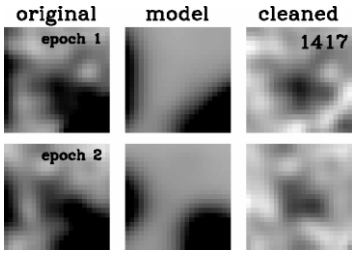

FIG. 2.—Examples of the deblending procedure in the IRAC 3.6 μm image as performed separately for the first (*top*) and second (*bottom*) epoch images from GOODS. We fit the original images (*left*) using the high-resolution NICMOS data to construct models for the nearby neighbors (*middle*) that are subtracted, resulting in the cleaned images (*right*). We recover consistent fluxes for both epochs after subtraction. The panel sizes are 4.″1 × 4.″1.

the spectral energy distributions (SEDs) are flatter at 1.1–2.2 and 3.6–4.5 μm (see Table 1). The rise at 3.6 μm is similar in strength to what is found in spectroscopically confirmed galaxies at $z = 6$ (Yan et al. 2005; Eyles et al. 2005) and suggests the presence of a substantial redshifted Balmer break, indicative of evolved stellar populations.

4. STELLAR POPULATIONS OF $z \approx 7$ GALAXIES

We fit stellar population synthesis models of Bruzual & Charlot (2003) and a Calzetti et al. (2000) obscuration law to the broadband fluxes to constrain the stellar populations. The models assume solar metallicity and a Salpeter initial mass function

TABLE 2
BEST-FIT MODEL PARAMETERS

ID	z_{phot}	Mass ($10^9\ M_\odot$)	Age$_w$ (Myr)	A_V	SFR ($M_\odot$ yr^{-1})	χ^2_{red}
Solar Metallicity						
Single-Age Burst (SSP)						
964	$7.2^{+0.1}_{-0.2}$	$1.8^{+0.7}_{-0.4}$	40	0.0	0.0	1.5
1417	$6.7^{+0.2}_{-0.2}$	$5.8^{+0.9}_{-1.0}$	81	0.1	0.0	0.8
950	$7.2^{+0.1}_{-0.1}$	$1.0^{+0.2}_{-0.1}$	25	0.0	0.0	1.4
1125	$7.0^{+0.2}_{-0.3}$	$0.7^{+0.4}_{-0.1}$	32	0.0	0.0	0.9
Exponentially Declining SFR (e-folding time $\tau = 100$ Myr; τ_{100})						
964	$7.2^{+0.1}_{-0.1}$	$3.4^{+0.8}_{-0.7}$	133	0.0	5.2	1.2
1417	$6.8^{+0.1}_{-0.2}$	$9.3^{+1.3}_{-2.2}$	176	0.2	10.7	0.7
950	$7.3^{+0.1}_{-0.2}$	$0.6^{+0.5}_{-0.3}$	35	0.0	9.4	1.1
1125	$7.1^{+0.1}_{-0.2}$	$0.9^{+0.8}_{-0.6}$	77	0.0	4.4	0.8
Constant Star Formation						
964	$7.4^{+0.1}_{-0.2}$	$4.2^{+2.4}_{-2.1}$	320	0.0	7.3	1.3
1417	$6.8^{+0.2}_{-0.2}$	$11.5^{+4.5}_{-3.6}$	254	0.4	25.5	0.9
950	$7.3^{+0.1}_{-0.2}$	$0.7^{+0.6}_{-0.4}$	40	0.0	9.9	1.1
1125	$7.0^{+0.2}_{-0.2}$	$1.0^{+1.3}_{-0.6}$	127	0.0	4.5	0.8

NOTES.—The best-fit parameters for Bruzual & Charlot (2003) stellar population models and a Calzetti et al. (2000) obscuration law. We omit the B and 8 μm band from the fit as they are not deep enough to constrain the models, leaving nine filters (V_{606}, i_{775}, z_{850}, J_{110}, H_{160}, K_s, 3.6 μm, 4.5 μm, and 5.8 μm), and four free parameters (redshift, stellar mass, age, and visual extinction A_V). We assume solar metallicity and a Salpeter IMF from 0.1 to 100 $M_\odot$; adopting a Chabrier IMF would result in similar ages but ~1.7 times lower stellar masses. Subsolar (1/50 $Z_\odot$) metallicities result in 30% higher ages and 20% higher masses. We consider redshifts from 0 to 10 and A_V from 0 to 2. We explore three SFHs: SSP, τ_{100}, and CSF. The 68% confidence intervals are obtained from Monte Carlo simulations, and the reduced χ^2_{red} values assume 5 degrees of freedom. We impose a minimum best-fit age of 25 Myr to avoid unrealistically young solutions. Finally, we weight the best-fit age with the SFH to better represent the age of the stars comprising the bulk of the stellar mass (age$_w$) For CSF the correction is 0.5, and for exponentially declining SFHs it is $[\text{age} - \tau + \tau \exp(-\text{age}/\tau)]/[1 - \exp(-\text{age}/\tau)]$, while SSP requires no correction (Förster Schreiber et al. 2004).

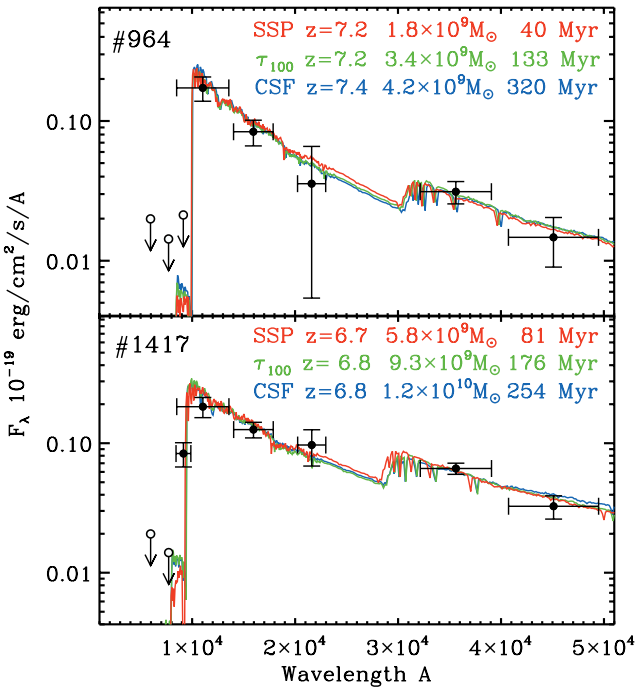

FIG. 3.—Observed SEDs of the IRAC-detected $z \approx 7$ galaxies and the best-fit solar metallicity models for each star formation history. The vertical and horizontal bars mark the 1 σ flux uncertainty and the width of the passband. The arrows are 1 σ upper limits. The sources show evidence for a break between the near-infrared and mid-infrared fluxes, which is well fit by a fairly evolved stellar population. The fits generally require little reddening, although galaxy 1417 also allows for moderate amounts of reddening and fairly large star formation rates (up to $A_V = 0.4$ and SFR ~ 25 $M_\odot$ yr^{-1}).

(IMF) between 0.1 and 100 $M_\odot$. We explore three different star formation histories (SFHs): a single-age burst (simple stellar population [SSP]), an exponentially declining star formation rate (SFR) with a timescale of 100 Myr (τ_{100}), and constant star formation (CSF). We leave the redshift, mass, age, and extinction as free parameters.

We find acceptable fits for all sources (see Table 2 and Fig. 3) and obtain confidence intervals on the parameters with Monte Carlo simulations. The best-fit redshifts vary from 6.7 to 7.4, and most Monte Carlo solutions are in a narrow range around the best fit, indicating that the redshift is well constrained. Old stellar populations at $z \sim 1$ fit the data poorly as they do not reproduce the strong break across the i_{775}, z_{850}, and J_{110} bands and the blue near-infrared continuum. Even so, we note that 3% and 11% of the solutions for object 1417 and 1125, allowed a redshift of $z \sim 1$ when the random flux variations "conspired" to suppress the break. The best-fit models have average rest-frame optical colors of $U - V = 0.4$ (0.2) and V-band luminosities $L_V = 2.3(1.0) \times 10^{10}\ L_\odot$ for the IRAC-detected (undetected) sources.

Determinations of the stellar population age and mass depend on the assumed star formation history and metallicity. For the whole sample, τ_{100} models fit the best, with ages of 40–180 Myr and instantaneous SFRs of 4–11 $M_\odot$ yr^{-1}. Converting the rest-frame 1500 Å luminosities directly into (absorption-corrected) SFRs (Madau et al. 1998) results in similar values. Nevertheless, the degeneracy between age and dust prevents us from placing firm limits on the ages and SFRs. The stellar masses are generally better constrained. As expected, the IRAC-detected galaxies 964 ($z_{ph} = 7.4$) and 1417 ($z_{ph} = 6.8$) are the reddest, most massive, and oldest in the sample. The average uncertainties on the masses are approximately a factor of 2–3.

The extreme SSP and CSF models set lower and upper boundaries to the masses, ages, and SFRs, whereas assuming subsolar metallicities (1/50 $Z_\odot$) instead of solar results in 30% higher ages and 20% higher masses. Because all SFHs and metallicities provide equally acceptable fits to the data, we hereafter adopt the mean of the SSP and CSF models and both metallicities as our fiducial values. We then find ages of 50–200 Myr, masses of (1–10) $\times$ 10^9 $M_\odot$, low reddening $A_V <$ 0.4, and star formation rates of 3–12 $M_\odot$ yr^{-1}.

5. DISCUSSION

Using the GOODS data set (M. Dickinson et al. 2006, in preparation), we have estimated and analyzed the *Spitzer* IRAC mid-infrared fluxes of four z_{850}-dropout candidates, which were identified in the HUDF by B04 and remeasured more accurately in BI06. The sources are rare, with a surface density of 0.7 arcmin^{-2}, and very faint, with observed magnitudes of $H_{160} = 26$–27 and 3.6 $\mu = 25$–27, placing them well beyond the spectroscopic capabilities of current telescopes but in reach of future facilities such as *James Webb Space Telescope* and Atacama Large Millimeter Array (ALMA). IRAC directly confirms the reality of two sources, while two others are marginally detected. Modeling of the broadband fluxes strongly supports their interpretation as $z \approx 7$ galaxies with substantial stellar masses (1–10) $\times$ 10^9 and ages 50–200 Myr.

Using the redshift selection function for the z_{850}-dropout sample (B04), we obtain an effective volume of 9000 Mpc^3 to $0.3L^*_{z=3}$, and we infer a stellar mass density of $\rho_* = 1.6^{+1.6}_{-0.8} \times 10^6$ $M_\odot$ Mpc^{-3}. Comparing this to the stellar mass density at lower redshifts, computed using similar techniques to similar luminosities, we find a continuing decrease where the density at $z \approx 7$ is 95%, 22% of that at $z = 6$, 5 (Yan et al. 2006; Stark et al. 2006). Recent smooth particle hydrodynamics (SPH) simulations in a ΛCDM universe predict stellar mass- and number densities for massive (>1.8 $\times$ 10^9 $M_\odot$) galaxies of 0.9 $\times$ 10^6 $M_\odot$ Mpc^{-3} and 2.5 $\times$ 10^{-4} Mpc^{-3} (SPH G6 run; Nagamine et al. 2005), remarkably close to the minimum estimates for our sample (0.7 $\times$ 10^6 $M_\odot$ Mpc^{-3} and 2.2 $\times$ 10^{-4} Mpc^{-3} to the same mass limit). However, we cannot exclude additional stellar mass residing in massive non–star-forming or dust-enshrouded galaxies, which the z_{850}-dropout criteria would have missed.

The ages of the two most massive (IRAC-detected) z_{850} dropouts suggest that the bulk of their stellar mass formed at even higher redshifts $z \gtrsim 8$, during the epoch of cosmic reionization (Spergel et al. 2006). We can place a simple upper limit on the contribution of high-mass galaxies to reionization by calculating the maximum SFR densities implied by the observed stellar masses and ages for these objects. Taking the maximum masses and dividing it by the minimum ages (~60 Myr), we infer a substantial SFR density 0.04 $M_\odot$ yr^{-1} Mpc^{-3}. This is higher than the density calculated directly from the rest-frame UV luminosities at $z = 6$–7 to the same limits (Bouwens et al. 2006b) but still more than 3 times too small to reionize the universe at the lowest probable redshift $z_{\rm reion} = 8.6$ (Spergel et al. 2006) for canonical assumptions (Madau et al. 1999; Bouwens et al. 2006b; see also Yan et al. 2006).

The simplest explanation for the lack of ionizing photons provided by high-mass galaxies at $z = 7$ is that low-mass galaxies beyond our current detection limits were primarily responsible for reionization (Lehnert & Bremer 2003; Yan & Windhorst 2004; Bouwens et al. 2006b). Other possibilities are that massive galaxies are missing from current surveys and are unaccounted for in the models, or that the observed galaxies had a top-heavy IMF, which would increase the ionizing efficiency per unit stellar mass. Obviously, incompleteness, sample variance, and large-scale structure dominate the uncertainties in our results. Larger, very deep near-infrared surveys from the ground and from space will address this issue in more detail.

We are most grateful for the efforts of the GOODS team who provided the data used in this analysis. We thank Ken Nagamine for providing his numerical simulations and the referee for helpful comments. I. L. is supported by a fellowship from the Carnegie Institution of Washington. R. B. and G. D. I. acknowledge support from NASA grant HST-GO09803.05-A and NAG5-7697.

REFERENCES

Bertin, E., & Arnouts, S. 1996, A&AS, 117, 393
Bouwens, R. J., & Illingworth, G. D. 2006, Nature, in press (astro-ph/0607087) (BI06)
Bouwens, R. J., et al. 2004, ApJ, 616, L79 (B04)
———. 2006b, ApJ, in press (astro-ph/0509641)
Bruzual, G., & Charlot, S. 2003, MNRAS, 344, 1000
Calzetti, D., et al. 2000, ApJ, 533, 682
Daddi, E., et al. 2005, ApJ, 626, 680
Dow-Hygelund, C. C., et al. 2005, ApJ, 630, L137
de Jong, R. S., et al. 2006, NICMOS Instrum. Sci. Rep. 2006-001 (Baltimore: STScI)
Eyles, L. P., et al. 2005, MNRAS, 364, 443
Fazio, G. G., et al. 2004, ApJS, 154, 10
Förster Schreiber, N. M., et al. 2004, ApJ, 616, 40
Franx, M., et al. 2003, ApJ, 587, L79
Labbé, I., et al. 2005, ApJ, 624, L81
Lehnert, M. D., & Bremer, M. 2003, ApJ, 593, 630
Madau, P., Haardt, F., & Rees, M. J. 1999, ApJ, 514, 648
Madau, P., Pozzetti, L., & Dickinson, M. 1998, ApJ, 498, 106
Mobasher, B., et al. 2005, ApJ, 635, 832
Nagamine, K., et al. 2005, ApJ, 627, 608
Papovich, C., Dickinson, M., & Ferguson, H. C. 2001, ApJ, 559, 620
Shapley, A. E., et al. 2001, ApJ, 562, 95
———. 2005, ApJ, 626, 698
Somerville, R. S., Primack, J. R., & Faber, S. M. 2001, MNRAS, 320, 504
Spergel, D. N., et al. 2006, ApJ, submitted (astro-ph/0603449)
Stark, D., et al. 2006, ApJ, submitted (astro-ph/0604250)
Steidel, C. C., et al. 1996a, AJ, 112, 352
———. 1996b, ApJ, 462, L17
———. 2004, ApJ, 604, 534
Thompson, R. I., et al. 2005, AJ, 130, 1
Yan, H., & Windhorst, R. A. 2004, ApJ, 600, L1
Yan, H., et al. 2004, ApJ, 616, 63
———. 2005, ApJ, 634, 109
———. 2006, ApJ, in press (astro-ph/0604554)